Title

Telencephalic outputs from the medial entorhinal cortex are copied directly to the hippocampus

Authors and Affiliations

Sau Yee Tsoi*, Merve Öncül*, Ella Svahn, Mark Robertson, Zuzanna Bogdanowicz, Christina McClure and Gülşen Sürmeli

*S.Y.T. and M.Ö. equally contributed to the study.

University of Edinburgh, Centre for Discovery Brain Sciences, Edinburgh, UK
G.S., S.Y.T., M.Ö., E.S., M.R., Z.B., C.M.
Simons Initiative for the Developing Brain
G.S.
Current addresses
University College London, UK
E.S.
NHS Greater Glasgow and Clyde, UK
M.R.
Vector Core, USA
C.M.

Abstract

Standard models for memory storage assume that signals reach the hippocampus from superficial layers of the entorhinal cortex (EC) and are returned to the telencephalon by projections from deep layers of the EC. Here we show that telencephalon-projecting cells in Layer 5a of the medial EC send a copy of their outputs back to the CA1 region of the hippocampus. Our results suggest that rather than serving as a relay, deep EC may coordinate hippocampal-neocortical interactions in memory consolidation.

Main

A central tenet of theories for systems memory consolidation is the interplay between the hippocampus and the neocortex[1,2]. Bidirectional communication between the neocortex and the hippocampus is mediated by the entorhinal cortex (EC), where the superficial and deep layers respectively channel inputs to and outputs from the hippocampus. In leading theoretical models, the deep layers of EC are considered as a relay of hippocampal output that reinstates neocortical activation patterns representing memories[2–5]. However, the segregation of hippocampal recipient and telencephalon-projecting neurons in the deep layers[6], and capacity of deep layers to integrate neocortical inputs with hippocampal output[7,8], suggest more complex roles[9]. An intriguing possibility, suggested by experiments with classic retrograde tracers, is that deep layers of EC also project to the hippocampus[10,11] implying that they have a dual function in coordinating neocortical and hippocampal networks. However, the targets of these hippocampus-projecting deep layer neurons, and their relationship to telencephalon-projecting deep layer neurons are unknown.

Layers 5a (L5a) and 5b (L5b) of the EC, are genetically distinct with differential input-output organisations. L5a but not L5b is the sole origin of the long-range telencephalic outputs of the EC[6], whereas L5b, but not L5a, is directly influenced by superficial layers of EC[6,8] and

inputs from the dorsal hippocampus preferentially target L5b over L5a[6,12,13]. To find out whether neurons in either L5a or L5b project to the hippocampus we injected a retrograde adeno-associated viral vector (AAV) expressing green fluorescent protein (GFP) into intermediate CA1. As well as finding retrogradely-labelled cell bodies in layer 3, which are well established as a critical input to stratum lacunosum of CA1[14], we also found labelled cell bodies in L5a, which we identified by immunostaining against the ETS variant transcription factor-1 (Etv1) protein, but not in L5b (Fig. 1a)[6]. Thus, projections from deep layers of EC to CA1 originate in L5a.

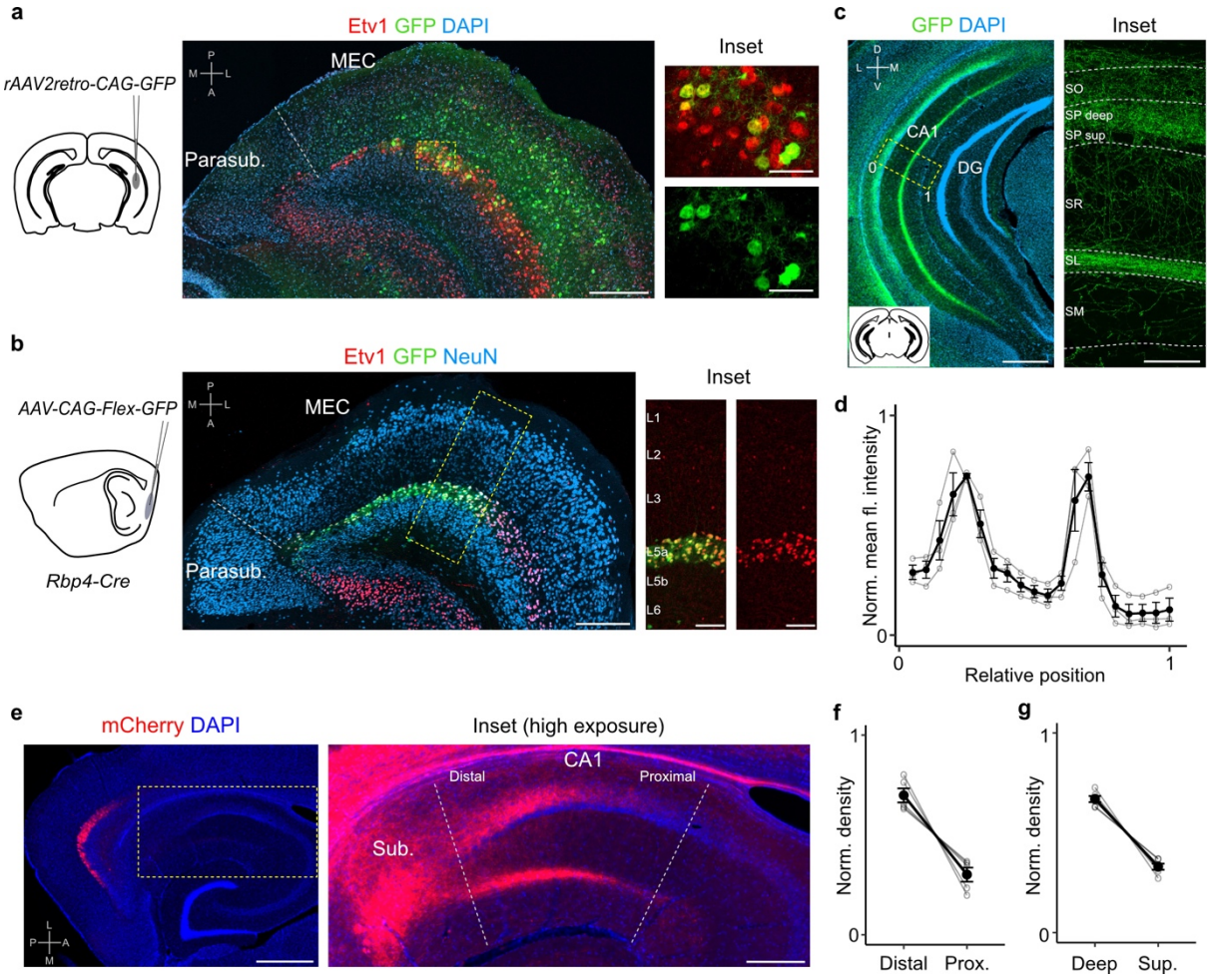

Figure 1. Origin and distinct topography of entorhinal deep layer projections to CA1
a, Left: a retrograde AAV virus was injected in the intermediate hippocampus. Middle: Entorhinal area on a horizontal brain section. Retrogradely labelled neurons were found in L3 as well as L5a, marked by Etv1 expression (Scale bar: 250 µm). Inset: high-magnification image of boxed region in left panel showing co-expression of GFP and Etv1 (Scale bar: 50 µm).
b, Left: *Rbp4-Cre* mice were injected in the deep MEC with a Cre-dependent virus expressing GFP. Middle: expression of GFP overlaps with expression of Etv1 (88.6%, n = 3 mice, 1866 cells; Scale bar: 250 µm). Inset: high-magnification of boxed region in middle panel (Scale bar: 100µm).
c, Coronal section showing the distribution of axons of MEC L5a cells in CA1 (Scale bar: 500 µm). Inset: high-magnification image of boxed region in left panel (Scale bar: 100 µm).
d, Quantification of fluorescence intensity across the layers of CA1. The area between 0 and 1 in **c** was divided into 20 bins, and the mean fluorescence intensity was calculated for each bin. Values shown are normalised mean fluorescence intensity values (n = 6 mice, 2 sections per brain).
e. Left: Horizontal section showing the injection site at low exposure. Right: A high exposure image from the hippocampal area of the same tissue showing the distribution of L5a axons across the proximal-distal axis of CA1 (Scale bar: 250 µm).
f. Normalised mean fluorescence density values in proximal versus distal CA1 (n = 5 mice).
g. Normalised mean fluorescence density values in deep versus superficial SP (n = 6 mice). Within SP, axon density in deep SP was significantly higher than density in superficial SP (paired one-tailed Wilcoxon signed rank test, p = 0.0156, effect size = 0.899, n = 6).

Cre)[15], that enables specific genetic access to L5a. Following injection of a Cre-dependent AAV expressing GFP or mCherry into the deep MEC of *Rbp4-Cre* mice, fluorescent signal was detected mainly in L5a (Fig. 1b and Extended Data Fig. 1a). The majority of labelled L5a neurons expressed Etv1 (88.6%, n = 3 mice, 1866 cells; Fig. 1b), similar to L5a neurons that were retrogradely labelled from the hippocampus (78.8%, n = 3 mice, 749 cells) or from cortical (89.2%, n = 8 mice, 2175 cells) and subcortical target areas (89.0%, n = 7 mice, 1771 cells; Extended Data Fig. 1b). Thus, like telencephalon-projecting L5a neurons, deep MEC neurons that project to the hippocampus are distinguished by expression of Etv1 and can be genetically accessed using *Rbp4-Cre* mice.

To what extent does the projection from L5a to CA1 differ from the previously identified projections arising from superficial layers of MEC? In contrast to projections from superficial MEC, which target either stratum lacunosum (SL) or stratum moleculare (SM) of CA1[16], axons from L5a neurons were primarily found in deep stratum pyramidale (SP) and stratum lacunosum (SL) but were sparse in stratum moleculare (SM) (Fig. 1c,d,e,g). Moreover, axons from L5a also differed in their proximo-distal organisation within CA1. Whereas projections from superficial layers of MEC favour proximal CA1[17], axons from L5a had highest density in distal CA1 (paired one-tailed Wilcoxon signed rank test, p = 0.0312, effect size = 0.905, n = 5; Fig. 1e,f and Extended Data Fig. 1c). This distinct topography suggests a unique functional role for the projections from L5a of MEC to CA1.

Our findings suggest two intriguing possibilities for the organisation of output neurons in L5a of the MEC. The hippocampus-projecting neurons in L5a may be distinct from the telencephalon-projecting neurons, implying separate processing within the deep MEC layers of signals to the hippocampus and telencephalon. Alternatively, the same neurons in L5a may project to both the telencephalon and the hippocampus, implying that telencephalic outputs from MEC are copied back to the hippocampus. To distinguish between these possibilities we used a combinatorial viral labelling strategy. We restricted reporter gene expression to subpopulations of L5a cells that project to specific targets by injecting a retrograde AAV expressing Cre recombinase in either the retrosplenial cortex (RSC) or nucleus accumbens (NucAcb), and a Cre-dependent fluorescent reporter virus into the MEC (Fig. 2a,b and Extended Data Fig. 2a,b,c,d,e). With this approach we detected in CA1 fluorescently-labelled axons originating from both RSC-projecting and NucAcb-projecting L5a neurons (Fig. 2c,d). The axon distribution across layers was similar to when L5a neurons were labelled in bulk using the *Rbp4-Cre* mouse line (Fig. 2e,f). These results establish the principle that axon projections from L5a of MEC to the hippocampus are collaterals of projections to telencephalic targets. However, it is unclear from these experiments whether this principle applies to projections from L5a to all of its many telencephalic targets.

Entorhinal cortex output projections are very diverse, covering the entire cortical mantle as well as basal ganglia and amygdala[18]. To test whether axon collateralisation to the hippocampus is a general feature of all telencephalon-targeting neurons, we used Multiplex Analysis of Projections by Sequencing (MAPseq)[19]. We injected the MAPseq barcode RNA virus library into the full dorso-ventral extent of the MEC (Extended Data Fig. 2f) and quantified barcode RNA expression in five major divisions of the brain (isocortex, cerebral nuclei (CNU), olfactory areas and cortical subplate (Olf/Ctxsp), dorsal and ventral hippocampus), as well as MEC, which we divided into a dorsal and ventral half (Fig. 2g). The majority of barcodes that were detected in any one of the three target divisions (isocortex, CNU or Olf/Ctxsp) were also detected in the hippocampus, suggesting that collateral axons to the hippocampus is a common feature of telencephalon-projecting neurons (Fig. 2h). The results were similar regardless of whether the neuron was located in dorsal or ventral MEC (Extended Data Fig. 2g), suggesting that collateralisation does not depend on the neuron's position in the dorso-ventral axis of the MEC. Using barcode counts as a measure of

projection strength[19] we further found that dorsal MEC neurons preferentially project to dorsal aspects of the hippocampus and ventral MEC neurons to the ventral aspects, indicating that the back-projections are topographically organised (Fig. 2i). Together these results reveal general organising principles by which all projections from MEC to the telencephalon are copied back to the hippocampus.

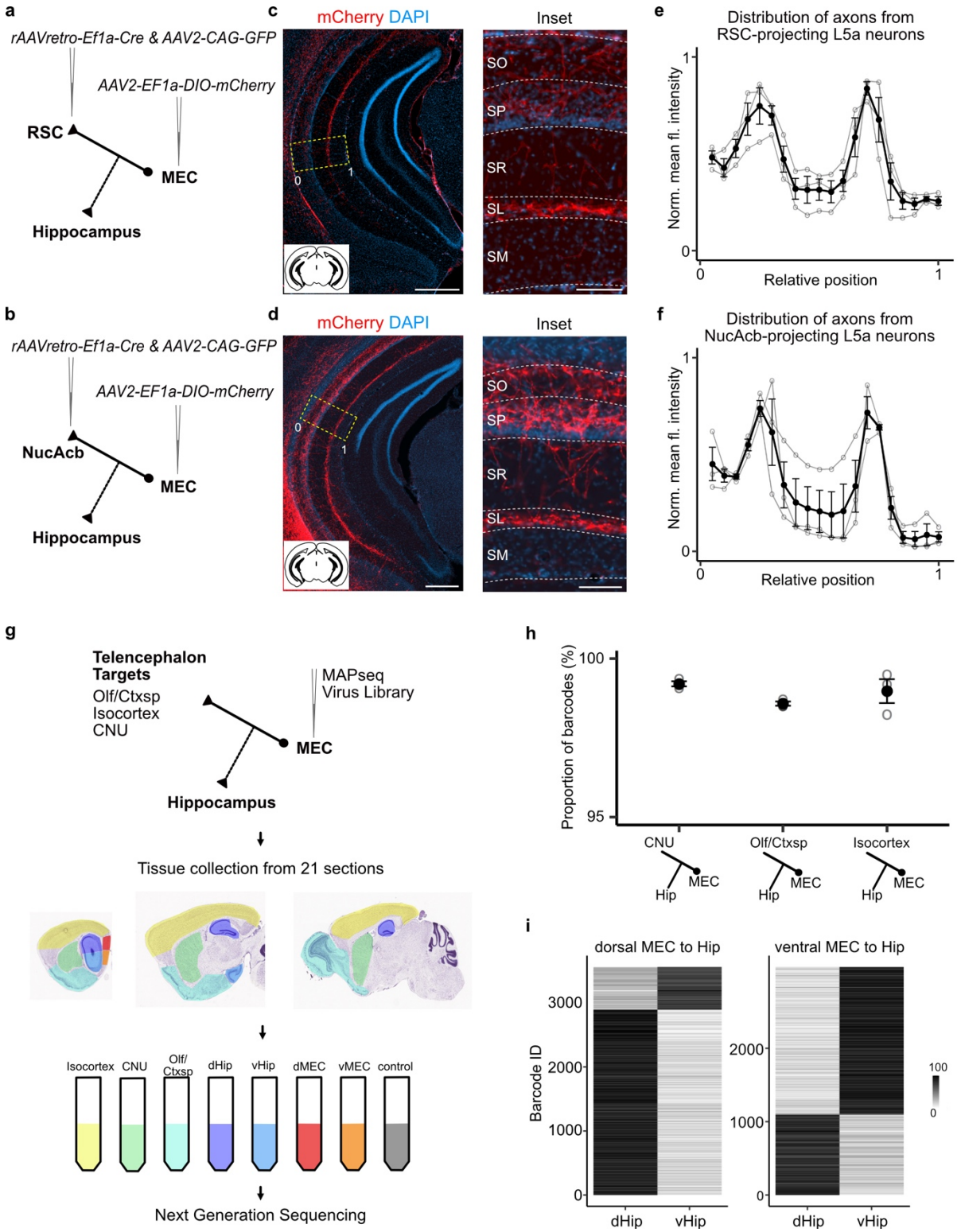

Figure 2. Telencephalic output of the MEC is copied to CA1
a, b, Experimental strategy. In wild-type mice, a retrogradely transported virus expressing Cre was injected in either the retrosplenial cortex (RSC; **a**) or nucleus accumbens (NucAcb; **b**), while a Cre-dependent reporter virus was injected in the deep MEC.
c, d, Hippocampal axon collaterals of RSC-projecting **(c)** or NucAcb-projecting MEC neurons (**d**; Scale bar: 250 µm). Inset: high-magnification image of boxed region in left panels showing distribution of axons across CA1 layers (Scale bar: 100 µm).
e, f, Quantification of mean fluorescence intensity across the layers of CA1 when only RSC-projecting (**e**) or NucAcb-projecting (**f**) MEC neurons were labelled (n = 3 mice for each group). Axon topography is similar to when L5a neurons are marked globally in the *Rbp4-Cre* line.
g, Experimental strategy. A MAPseq virus library was injected into deep MEC (n = 3). 44hrs later, mice were sacrificed and brains were sectioned sagittally at 400 µm thickness. Tissue from 5 major divisions (Isocortex, CNU, Olf/Ctxsp, dHip and vHip), as well as dorsal and ventral MEC were then dissected and collected in tubes. Brainstem tissue was collected as a negative control. Tissue was further processed for RNA extraction and next generation sequencing.
h, Nearly all barcodes detected in CNU, Olf/Ctxsp and Isocortex were also detected in the hippocampus (Isocortex: 98.6% ± 0.06%; CNU: 99.2% ± 0.08%; Olf/Ctxsp: 99.0% ± 0.4%; n = 3 mice, 5358 barcodes).
i, Dorso-ventral topography of projections revealed by relative barcode counts. For each barcode, counts were normalised to show the relative projection strength of each neuron to dorsal and ventral hippocampus (n = 3 mice).

Which cell types within the hippocampus receive signals from L5a of MEC? While the compartmentalised arrangement of axons from L5a of MEC suggests selective targeting of CA1 layers, axonal topography does not necessarily reflect functional connectivity. Therefore, we targeted viral vectors expressing a channelrhodopsin2-mCherry conjugate to L5a neurons in MEC and tested for connectivity using whole-cell ex-vivo patch clamp recordings from CA1 neurons (Fig. 3a and Extended Data Fig. 3a,b).

We focus initially on responses of pyramidal cells. Brief light pulses evoked depolarising sub-threshold postsynaptic potentials (PSPs) in 64% of SP pyramidal neurons recorded at their resting membrane potential (Fig. 3b,c and Extended Data Fig. 3e). The response probability of neurons in distal CA1 was not significantly different than neurons in proximal CA1 (Fig. 3d). The majority of PSPs (20 out of 26) maintained their polarity when the membrane potential was adjusted from rest (Vm = -66.7 ± 0.6) to -50 mV, indicating that they were glutamatergic. Consistent with this, in these neurons EPSPs were maintained when $GABA_A$ receptors were blocked with Gabazine, but were abolished by the AMPA receptor antagonist NBQX, demonstrating that they are glutamatergic (Fig. 3e). The responses had short latencies (3.04 ± 0.26 ms, n = 20 cells, 15 mice) that were relatively invariant from trial to trial (Fig. 3f) and were independent of the response's position within a train of stimuli, indicating that they are monosynaptic (Extended Data Fig. 3f). Moreover, responses were sensitive to bath application of tetrodotoxin (TTX) but recoverable after application of 4-Aminopyridine (4-AP; Fig. 3g)[20]. Together, these data demonstrate that projections from L5a of the MEC provide glutamatergic excitatory inputs directly to pyramidal neurons in proximal and distal CA1.

A smaller population of pyramidal neurons showed PSPs with characteristics of indirect inhibitory connections. These responses either reversed polarity when the cell was held above the chloride reversal potential (Fig. 3h) or had an early depolarising and a late hyperpolarising component (Extended Data Fig. 3d). Application of Gabazine either completely blocked the PSPs (Fig. 3i) or revealed a larger excitatory component that was sensitive to application of NBQX (Extended Data Fig. 3d). Thus, inputs from L5a of the MEC also recruit local interneurons that provide inhibitory input to SP pyramidal neurons.

To identify which interneurons in CA1 were targets of L5a projections, we tested responses of interneurons in all layers. In SP we distinguished interneurons from principal cells either by classifying them based on biophysical properties (fast-spiking: SP_{FSInt} and non-fast spiking:

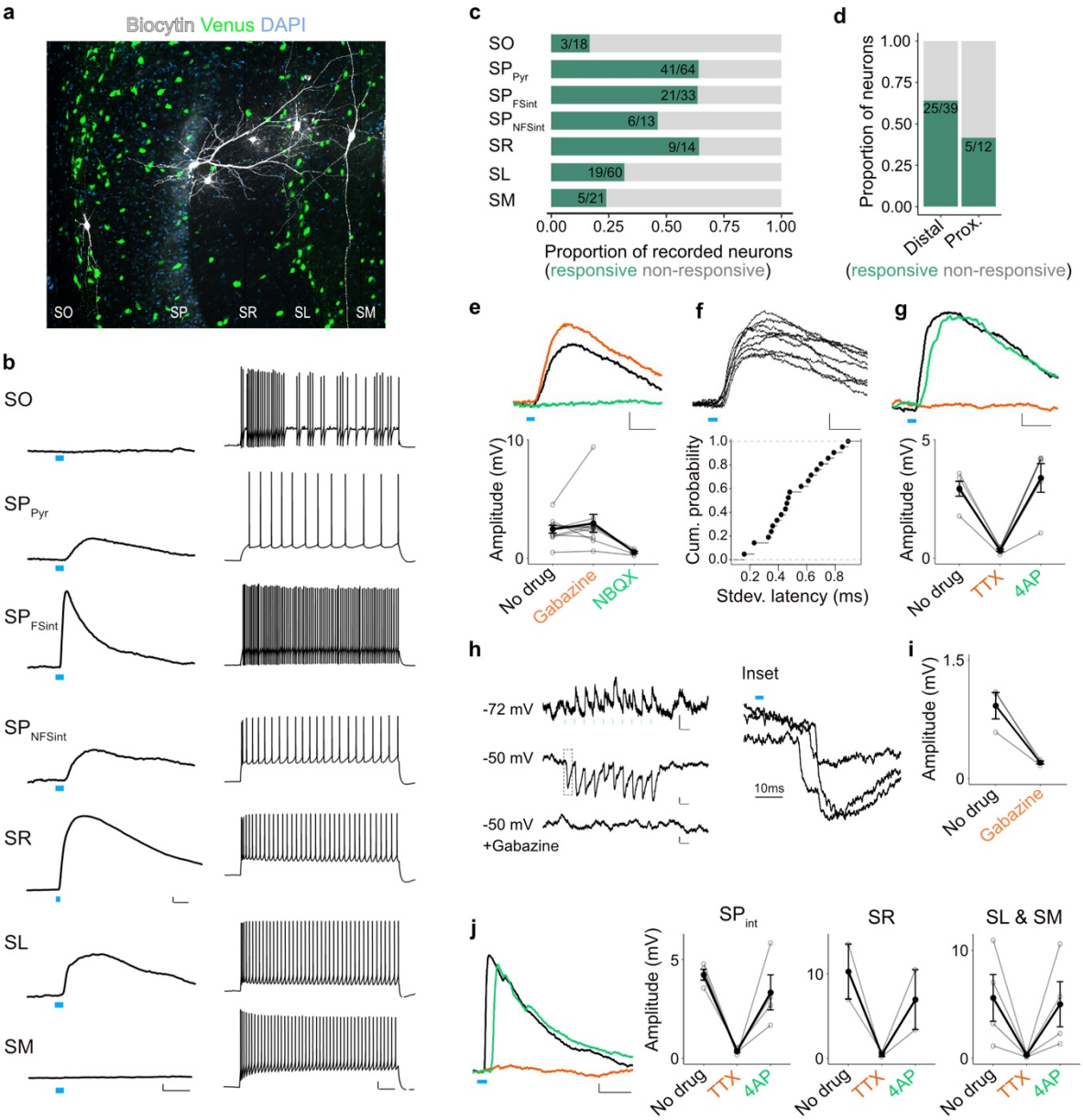

Figure 3. L5a neurons of the MEC target distinct neuronal populations in CA1.
a, An example confocal image showing interneurons marked by the expression of venus fluorescent protein driven by the vesicular GABA transporter (*Vgat*) gene's promoter and biocytin filled neurons in the *Rbp4-Cre X Vgat-Venus* double transgenic mouse line. Fluorescent labelling facilitated patch-clamp recordings made from GABAergic interneurons and distinguishing SR, SL and SM.
b, Left: Representative examples of depolarising responses recorded at resting membrane potential following 3 ms blue light stimulation (blue line) of L5a axons in CA1 (Scale bar: 1 mV, 10 ms). Neurons in SO and SM were typically not responsive (< 30%). Responses from SR neurons were on average larger than the responses from neurons in other layers (Scale bar: 1 mV, 10 ms). Right: Neurons' spiking response to injecting 200 pA current (Scale bar: 10 mV, 100 ms)
c, Proportion of responsive neurons in all layers of CA1 recorded at resting membrane potential. Green highlighted segment corresponds to the proportion of cells with depolarising membrane potentials; grey highlighted segment corresponds to neurons with no change in their membrane potential.
SO: n = 18 cells, 10 mice; SP_{Pyr}: n = 64 cells, 27 mice;
SP_{FSint} : n = 33 cells, 8 *Rbp4-Cre X Pvalb-Flp mice*, 5 *Rbp4-Cre X Vgat-Venus mice*, 8 *Rbp4-Cre* mice;
SP_{NSFint}: n = 13 cells, 11 *Rbp4-Cre* mice, 1 *Rbp4-Cre X Vgat-Venus* mouse;
SR: n = 14 cells, 6 mice; SL: n = 60 cells, 15 mice; SM: n = 21 cells, 10 mice.
d, Proportion of responsive pyramidal neurons located in the distal and proximal halves of CA1. The difference in proportions was not significant (X-squared = 1.0932, df = 1, p-value = 0.2958, Chi-squared test, n = 12 cells in proximal and n = 39 cells in distal CA1).

e, Effects of bath application of Gabazine (orange, n = 10 cells, 9 mice) and NBQX (green, n = 5 cells) on PSPs recorded from a pyramidal neuron (Scale bar: 0.5 mV, 10 ms) and a summary plot of PSP amplitude measurements for all tested pyramidal neurons. Note that some neurons were only treated with Gabazine which did not cause a significant change in amplitudes (p = 0.97, 2-tailed Student's t-test, n = 10 cells, 9 mice).
f, An example of ten consecutive PSP responses recorded from a single pyramidal neuron illustrates the short and invariant latency of PSPs (Scale bar: 0.5 mV, 10 ms) and a cumulative probability plot of standard deviation of latencies for neurons with PSP responses that were > 1 mV in amplitude (n = 20 cells).
g, Effects of bath application of TTX (orange) and 4-AP (green) on PSPs recorded from a pyramidal neuron (Scale bar: 0.5 mV, 10 ms) and a summary plot of changes in PSP amplitudes for all tested pyramidal neurons. TTX application abolished responses (n = 5 cells, 5 mice, p = 0.01, 2-tailed Student's t-test).
h. An example inhibitory PSP response recorded from a pyramidal neuron upon 10 Hz light stimulation (blue bars). Response polarity reversed when the neuron's membrane potential was adjusted to -50 mV and was abolished after application of Gabazine (Scale bars: 0.2 mV, 100 ms). Inset shows the long latency (> 10 ms) of PSP onset indicating polysynaptic connectivity.
i. Effects of bath application of Gabazine on the response amplitude of long latency PSPs (n = 3 cells).
j. Effects of bath application of TTX (orange) and 4-AP (green) on the response amplitude PSPs recorded from interneurons across CA1. Left: Example traces from a fast-spiking pyramidal layer interneuron (Scale bar: 1 mV, 5 ms). Right: summary plots of response amplitude measurements from multiple recordings (SP_{int}: n = 4, SR: n = 2, SL: n = 3, SM: n = 1 cells).

SP_{NSFint}; Extended Data Fig. 3f and see methods), or by recording from fluorescently-labelled GABAergic or parvalbumin-expressing (PV+) inhibitory neurons in double transgenic mice (Extended Data Fig. 3a,b,c). Stimulation of L5a axons elicited both sub-threshold and supra-threshold responses primarily in SP, SR and SL interneurons (Fig. 3b,c and Extended Data Fig. 3e). Depolarising PSPs were observed in 64% of the SP_{FSint} including PV+ ones, 46% of the SP_{NSFint}, 64% of SR and lower proportions of recorded neurons in SL (31%), SM (23%) and SO (16%). With the exclusion of SO, PSPs in all layers showed characteristics of monosynaptic connectivity (Fig. 3j) and AMPA receptor-mediated glutamatergic synaptic transmission (Extended Data Fig. 3g,i). Therefore, projections from L5a of MEC recruit CA1 interneurons through monosynaptic inputs driven by excitatory glutamatergic synapses.

Together our results suggest a substantial revision to the idea that the entorhinal deep layers unidirectionally convey hippocampal output messages to the neocortex. We show that L5a axons bifurcate to target both the telencephalon and CA1. These projections have a distinct topographical organisation in CA1 compared to projections from superficial layers. The exclusive L5a origin of this pathway reinforces the distinct input-output organisation of the deep MEC. While L5b is a point of integration for local and neocortical input with hippocampal output and distributes its signals locally within MEC, L5a appears to be suited to coordinate the wider hippocampal-neocortical loop by providing a copy of fully processed hippocampal output onto CA1. These output copies might provide a gating signal to modulate the impact in CA1 of inputs from CA3 and/or neocortical return inputs via L3 of EC[21]. It is conceivable that they influence mechanisms of learning and memory by affecting rhythmic network activity through the inputs on the pyramidal cells and interneuron populations that we described here[22].

Methods

Mice

All animal experiments were approved by the University of Edinburgh animal welfare committee and were performed under a UK Home Office project license. The *Rbp4-Cre* mouse line was generated by GenSat and obtained from MMRRC (*Tg(Rbp4-cre)KL100Gsat/Mmucd*). The *Vgat-Venus* mouse line was generated by Dr. Atsushi Miyawaki at RIKEN, Wako, Japan[23]. The *Pvalb-Flp* mouse line was obtained from Jackson Laboratories *(B6.Cg-Pvalb-tm4.1(FlPo)Hze/J; Jax 022730)*. Wild-type mice were obtained from Charles River Laboratories C57Bl6J stock. Double transgenics were generated by crossing the *Rbp4-Cre* line to the *Vgat-Venus* or the *Pvalb-Flp* lines. *Rbp4-Cre* and *Pvalb-Flp* lines were maintained as heterozygous and all mice were on C57Bl6 background.

Viral constructs and injection strategy

8 to 14 week-old male and female mice were used in all experiments. For targeting deep MEC a craniotomy was made 3.4 to 3.65 mm lateral to the bregma (X) between the transverse sinus and lambdoid suture (Y = 4.5 to 5 mm caudal to bregma). The injection pipette was at a 9 degree angle caudal to the dorsoventral plane (See Fig. 1b). 100 nl of virus was slowly released at four Z-depths 3.0, 2.8, 2.6 and 2.4 mm from the surface of the brain. 3 mins after delivering the virus the injection needle was retracted to the next injection depth until the most dorsal location where 10 mins past before the needle was fully retracted. For anterograde tracing of L5a axons *AAV-EF1a-DIO-mCherry* (serotypes 2 and 5, titer 5.3 x 10^{12}, lot #AV4375H, K., Deisseroth, UNC Vector Core) and *AAV-CAG-FLEX-GFP* (titer 3.7 x 10^{12}, lot #AV4530B, E. Boyden, UNC Vector Core) were used.

For injections in CA1 a craniotomy was made 3.5 mm lateral and 3.30 mm caudal to the bregma in C57BL6J mice. 100nl virus was delivered at 3.0, 2.8, 2.6, 2.4 and 2.2 mm from the surface. For retrograde labelling of hippocampus-projecting EC neurons, 100nl of a *rAAV2retro-CAG-GFP* (titre 4.3 x 10^{12}, lot #AV6951B, E. Boyden, UNC Vector Core) was injected at each depth.

To assess whether telencephalic projection neurons in L5a of MEC co-express Etv1 (Extended Data Fig. 1b), fluorophore coupled choleratoxin beta subunit (CTB-Alexa 488 and CTB-Alexa 555) was injected at various sites in wild-type C57BL6J mice as previously described[8].

To achieve Cre expression in target specific subpopulation of L5a neurons in the MEC (Fig. 2) a *rAAVretro-EF1a-Cre-WPRE* (viral construct was a gift from Karl Deisseroth, titre 2.4 x 10^{12}) was made using an AAV-retro helper plasmid (Addgene plasmid ID 81070) as described previously[24]. A cocktail of *rAAVretro-EF1a-Cre-WPRE* and *AAV-CAG-GFP* (titer 4.3 x 10^{12}, lot #AV6951B, Boyden, UNC Vector Core) viruses were injected either in NucAcb (X: +1.0 mm; Y: +1.2 mm; Z: -3.8, -4.0 mm) or RSC (X: +0.4 mm; Y: -2.8, -3.2 mm; Z: -0.9 mm) in wild-type mice. A Cre inducible reporter virus was also injected in the MEC as described above. GFP expression driven by the *CAG* promoter at the target site was used for verification of injection location.

To achieve expression of channelrhodopsin-2 in L5a axon terminals, we injected *AAV2-EF1a-DIO-hChR2(H134R)-mCherry-WPRE-pA* (titer 5.1 x 10^{12}, lot #AV4319J, Deisseroth) in the MEC of the *Rbp4-Cre* or the *Rbp4-Cre X Vgat-Venus* double transgenic mice. Additionally, in order to fluorescently label parvalbumin expressing interneurons in CA1 a Flp recombinase-dependent AAV vector was constructed in house and injected in the

hippocampus (X: +3.0 mm; Y: -3.5 mm; Z: -2.0, -3.0 mm, 200 nl virus was injected at each Z-depth). To produce the virus, the viral construct pAM-FLEX-GFP[25] (a gift from Peer Wulff) was used as the viral backbone. The eGFP, loxP and lox2272 sites were removed and replaced with a synthesised cassette (GenScript) containing a multiple cloning site flanked by two sets of heterotypic (FRT and F3), antiparallel FRT sites to produce pAM FLPX. For pAM FLPX eGFP and pAM FLPX mCherry, the fluorescent proteins were amplified from pAM FLEX eGFP and pmCherry-C1 (Clontech) respectively, with EcoRI and SacI overhangs and cloned into pAM FLPX. All AAV preps were generated in house as previously described[24] and were titered by qPCR following expression in HEK cells (> 10^{12} genome copies (GC)/ml).

The spread of viral expression was assessed from the fluorescent signal in all sections for each brain. Brains in which labelled neurons were found outside L5 were excluded; this was a result of occasional and sparse labelling in L2 or L3 or the parasubiculum.

Tissue processing and immunohistochemistry

3 to 4 weeks after the virus injection surgery, mice were transcardially perfused with 4% paraformaldehyde as previously described[6]. Brains were sectioned at 60 µm using a cryostat (Leica CM3050 S) either coronally or horizontally and sections were stored in PBS at 4°C. All subsequent incubation and washing steps were carried out at 4°C. Prior to antibody staining, sections were blocked with either 5% normal goat serum (NGS; Abcam: ab13970) or 2% bovine serum albumin (BSA; Sigma: A9418) in 0.3% PBST (PBS with 0.3% Triton-X100) for 2hrs. Sections were then transferred to primary antibody solutions made with either 5% NGS or 2% BSA in 0.3% PBST and incubated overnight. After 3 washes, each 20 min, in 0.3% PBST, sections were transferred to secondary antibody solutions made with 0.3% PBST and, if required, NeuroTrace 640/660 (1:800; Life Technologies: N21483) and incubated overnight. After 3 washes, sections were incubated in DAPI (1:2,000; Sigma Aldrich: D9542) solution made in PBS for 20 min at room temperature, where required, and then mounted on microscope slides using Mowiol® 4-88 (Aldrich: 81381). Slides were covered with glass coverslips and left to dry overnight at 4°C in the dark. The following primary antibodies were used: rat anti-mCherry (1:2,000; ThermoFisher: M11217), chicken anti-GFP (1:10,000; Abcam: ab13970), rabbit anti-Etv1[26] (1:1,000), chicken anti-NeuN (1:1,000; Sigma Aldrich: ABN91). All secondary antibodies were obtained from Invitrogen and used at a concentration of 1:800.

Cell counting

Every 4th brain section was imaged as a Z-stack (1 µm step size) using either the Zeiss LSM 800 or Leica SP8 confocal microscope at 20x magnification. Regions of interest were drawn around L5a and cell counting was carried out either manually using Fiji software, or using cell-counting tools in Vision4D (Arivis).

The boundaries for L5a were determined using either a DAPI or Neurotrace counterstain. The border between medial and lateral divisions of EC was determined in each section using layer 2 as a guide – in lateral EC, layer 2 is separated into two distinct layers, while this separation is not seen in medial EC[27].

Quantification of the distribution of fluorescent signal

Quantification of fluorescence across the radial axis of the CA1

The distribution of axons of L5a neurons in the radial axis of the hippocampal CA1 was quantified in slide-scanner images (Fig. 1) or confocal images (Fig. 2) using Fiji software. Coronal brain sections between 3.28 to 3.58 mm posterior to Bregma, which contain distal CA1, were selected for analysis. 2 sections from each brain in which the fluorescent labeling was representative of all the sections were used. DAPI was used as a counterstain. In each section, a 400 µm-wide rectangular ROI was drawn across the radial axes, covering all layers of a randomly selected region in intermediate CA1 (Fig. 1c). This ROI was then divided into 20 equal bins and the mean fluorescence intensity was calculated for each bin. The mean intensity values were then normalised in each brain by scaling the values such that the highest value is 1.

Quantification of fluorescence in the transverse axis of the CA1

A Zeiss Axioscan slidescanner was used to image every second brain section at 10x magnification. The projection strengths of MEC L5a neurons to proximal and distal halves of CA1 were quantified in horizontal sections located at depths between 2.56 mm to 4.12 mm from the surface of the brain, with injection sites located across medial, mid and lateral MEC (15-18 brain sections per mouse, n = 5 mice). GFP and mCherry fluorescence signals were amplified with immunostaining as described previously. The borders of CA1 were drawn on brain section images using a customisable digital microscopy analysis platform (Visiopharm), and the proximo-distal border was defined as the border equidistant from the proximal and distal ends of CA1. The mean fluorescence density, defined as the total number of pixels above a set threshold in an area divided by the total number of pixels in the area, was measured in proximal and distal CA1. The threshold was determined manually by ensuring that only pixels representing axons were detected as signal. A median unsharp background correction was used to remove background noise from axons outside of the focus plane of the image. The mean fluorescence density values were then normalised within each brain by scaling the values such that the total fluorescence density value (proximal + distal) in each brain is equal to 1.

MAPseq

5 C57Bl6J adult male and female mice were injected in the deep MEC with the MAPseq Sindbis viral barcode library (3 x 10^{10} GC/ml) provided by the MAPseq facility (Cold Spring Harbor Laboratories). To cover the whole mediolateral and dorsoventral extent of the MEC virus was injected in two locations: 3.4 mm and 3.6 mm lateral to bregma. 100 nl virus was delivered to 3.0, 2.8, 2.6, 2.4 mm below the surface of the brain. After 44 hrs, mice were sacrificed, brains were extracted and immediately immersed in oxygenated cold ACSF prepared in ultrapure water. All surgical tools and surfaces were treated with RNaseZAP (Invitrogen) prior to the start of the experiment and in-between samples. 400 µm fresh sagittal brain sections were cut using a vibratome[28]. Immediately after this, GFP expression in the deep EC was verified under a fluorescent microscope and tissue was dissected in cold oxygenated ACSF using microdissection blades on sylgard covered petri dishes which were kept on ice. Each slice was dissected on a previously unused surface of the plate with fresh ACSF and a dedicated microblade was used for the dissection of each brain division to prevent contamination. Tissue pieces were collected into bead containing (Qiagen 69989) collection tubes (Qiagen 19560) on dry ice. After tissue collection, 400 µl Trizol (Thermo Fisher Scientific #15596026) was added to each collection tube. The procedure was repeated for all 5 brains. 3 brains with the largest coverage of MEC deep layers were selected to proceed to the next steps. Tissue was stored at -80 degrees before it was shipped on dry ice to CSHL MAPseq core facility for further processing. RNA extraction, production of double stranded cDNA, library preparation and Illumina sequencing and preprocessing of sequencing data was performed by the MAPseq core facility as described in[19].

For the tissue dissections, identification of brain areas was done by using Allen Brain Reference Atlas (https://mouse.brain-map.org/). The isocortex division included the somatosensory, motor, visual, posterior parietal, anterior cingulate and retrosplenial areas combined. The cerebral nuclei (CNU) division was restricted to striatum. The olfactory/cortical subplate division (Olf/Ctxsp) was a combination of olfactory areas and cortical subplate including amygdalar nuclei. The remaining two divisions were dorsal (dHip) and ventral hippocampus (vHip) including subiculum. Some brain areas were excluded from the study because of the difficulty in dissecting or identifying brain areas in the sagittal plane. All sections > 3.7 mm lateral to bregma which are not annotated in Allen Brain Reference Atlas were excluded. Therefore, neocortical areas in the most lateral sections such as perirhinal cortex, ectorhinal cortex, temporal association areas were not included in the study. The claustrum and adjacent neocortical areas (visceral, agranular insular, gustatory) were excluded as it was not possible to separate these areas precisely to prevent contamination between the assigned divisions. Since borders between the brain divisions CNU and OLF/Ctxsp were not always clear, dissections avoided these areas hence the brain areas in these divisions are partially included. White matter between the hippocampus and the neocortex carrying axon tracts were also excluded. Brainstem and cervical spinal cord tissue were used as control. When L5a neurons in the MEC were labelled using strategies explained in Fig. 1, no axonal projections to these areas were observed (unpublished experiments). Consistent with this, a low number of barcodes were identified in the negative control samples (on average 1.0% of barcodes had counts in control areas, n = 3).

A limitation of the barcode-based single-cell tracing method comes from the possibility of multiple neurons being represented by the same barcode. This is prevented by adjusting the barcode diversity and the size of the target population as explained in detail in [19]. In order to assess the expected fraction of uniquely labelled neurons in our study we counted the total number of neurons in L5a of the MEC. A total of 2314 (± 131, n = 2 mice) NeuN-labelled neurons were counted. Using the formula $F = (1-(1/N))^{k-1}$ where N is the barcode diversity (2×10^6)[19] and k is the number of infected neurons the predicted ratio of uniquely labelled neurons is 99.9%. Multiple representation of neurons due to a neuron being infected by several different barcode RNA-expressing viral particles was not corrected for since the projection patterns are not affected by overrepresentation of neurons[19].

MAPseq data analysis

Barcode counts were first normalised in each area by the relative number of spike-in RNAs for each sample. Orphan barcodes, barcodes which did not have counts in the injection site, (dMEC or vMEC) were removed. We then calculated the 95th percentile of the barcode counts in our negative controls and based on this set all barcode counts of 1 to 0. A small number of barcodes had a higher count in any target area compared to the injection site which might be a result of incomplete dissection of the injection site or viral expression in areas that the virus spilled into as we retracted the pipette. These barcodes were removed. Since our goal was to find whether neurons projecting to the telencephalon also project to the hippocampus we removed the barcodes that had no counts in any of the telencephalic target areas. For the same reason, barcodes that were detected only in the dHip or vHip hippocampus were also removed. Finally, we excluded all barcodes with counts of less than 400 in the injection site to minimise the possibility of incomplete transport of RNA barcodes to axons in target areas due to weak expression at the cell bodies or low counts due to PCR or polymerase errors. Barcodes with low counts in all target areas (< 10) were also excluded to account for potential false positives.

To quantify the proportion of barcodes that were present in both a target division (Fig. 2h; Isocortex, CNU or Olf/Ctxsp) and the hippocampus, the following formula was used: (total number of barcodes with counts detected in both hippocampus and target division/total number of barcodes with counts detected in target division). To compare the difference between barcodes with the injection site in dMEC vs vMEC, the barcodes were divided into two groups – “dorsal MEC”, where counts in dMEC were higher than in vMEC, and vice versa for “ventral MEC”. A paired two-tailed Wilcoxon signed rank test was used to check if there was a significant difference between the proportion of collateralising neurons in dMEC and vMEC.

To visualise the distribution of barcode counts in dHip and vHip from “dorsal MEC” or “ventral MEC” groups, we generated heat maps showing normalised projection strengths between dHip and vHip for all barcodes. The normalised projection strengths were calculated by the formula: $\text{projection strength}_{dHip} = (\text{counts}_{dHip}) / (\text{counts}_{dHip+vHip}) * 100$, and likewise for vHip. Barcodes were sorted by maximum projection site.

Ex-vivo electrophysiology

Slice preparation

3 to 4 weeks after the injection of the viral vectors ex-vivo brain slices were prepared. Following decapitation, brains were immersed for 2 mins in 4°C artificial cerebrospinal fluid (ACSF) of the following composition (mM): 86 NaCl, 1.2 NaH_2PO_4, 2.5 KCl, 25 $NaHCO_3$, 25 Glucose, 75 Sucrose, 0.5 $CaCl_2$, 7 $MgCl_2$, bubbled with 95% O_2 / 5% CO_2. They were then sectioned horizontally (400 µm) using a vibratome (Leica VT1200) ACSF. Tissue was collected and maintained in extracellular solution of the following composition (mM): 124 NaCl, 1.2 NaH_2PO_4, 2.5 KCl, 25 $NaHCO_3$, 20 Glucose, 2 $CaCl_2$ and 1 $MgCl_2$, continuously supplied with 95% O_2 / 5% CO_2. Slices were allowed to rest for 15 mins at 35°C followed by a minimum of 30 mins recovery time at room temperature before the start of the experiment.

Electrophysiological recordings

Whole-cell patch-clamp recordings were made in pyramidal neurons and interneurons in all layers of hippocampal CA1. Typically, 2 to 3 slices from the intermediate hippocampus were used where morphologies of the pyramidal cells and interneurons were confirmed to be intact with post hoc staining and imaging of biocytin filled neurons.

Pipettes with 4 to 6 MΩ resistance were pulled from borosilicate glass (Sutter Instruments) and filled with an intracellular solution of following composition (mM): 130 K Gluconate, 10 KCl, 10 HEPES, 2 $MgCl_2$, 0.1 EGTA, 2 Na_2ATP, 0.3 Na_2GTP, 10 NaPhosphocreatine, 5.4 Biocytin. The intracellular solution was adjusted to a pH of 7.2 to 7.4 with KOH and osmolarity 290-300 mOsm. All recordings were made in current clamp mode with pipette capacitance neutralisation and bridge balance applied. Subthreshold membrane properties were measured from the changes in membrane potential upon depolarising and hyperpolarising current injections (typically -40 pA to +40 pA, in 20 pA). Rheobase was established from responses to a depolarizing current ramp (50 pA/sec, maximum current 400 pA).

For optogenetic stimulation of ChR2, an LED of wavelength 470 nm (ThorLabs) was attached to the epifluorescence port of the microscope. Where necessary, the irradiance of the LED (max 9 mW) was controlled by voltage commands. Pharmacological tests were done by bath application of the following reagents with the indicated final concentrations in

standard extracellular solution: Gabazine (10 µM, Hello Bio, Cat. No. HB0901), NBQX (10 µM, Tocris, Cat. No. 0373), D-AP5 (50 µM, Tocris, Cat. No. 0106), 4-AP (200 µM, Tocris, Cat. No. 0940), TTX (1 µM, Hello Bio). To allow for morphological reconstructions cells were filled with Biocytin (5.4 mM in intracellular solution, Sigma, Cat. No. B4261) during electrophysiological recordings.

Analysis of electrophysiological recordings

Electrophysiological properties were analysed using built-in and custom routines in IGORpro (WaveMetrics) and MATLAB. All basic properties were established from the I-V protocol described above. Input resistance was determined from the largest depolarising current step injected. Sag ratio was calculated as $V_{steady\ state}$/ V_{min} from the largest hyperpolarising current step. Rheobase and action potential (AP) threshold were determined from the first AP during injection of steadily increasing current in a ramp. From the same protocol, after-hyperpolarisation (AHP) was calculated as the difference between AP threshold and the most negative peak of the hyperpolarisation following the first spike. Half-width was measured as the width of the AP at half its maximum spike amplitude. Firing frequency was measured from a 1 s current injection of 200 pA. Maximum firing frequency was measured between the first two APs, and base frequency between the last two APs in a train.

For optogenetic stimulations, responsiveness was confirmed for each cell by a significant difference between the detected peak of change in membrane potential after light stimulation and the average baseline using a 2-tailed, type 1 student's t-test. The PSP amplitude and latency were measured using the Neuromatic toolbox in IGORPro.

Cell types were determined based on biophysical properties extracted from electrophysiology data. Pyramidal cells were identified from a max firing frequency of < 50 Hz, AHP < 10 mV, AP half-width ≥ 0.7 ms and sag ≤ 0.9, with descending hierarchical order. Fast spiking interneurons were categorised from a max firing frequency ≥ 100 Hz, AHP ≥ 12 mV, AP half-width < 0.5 ms and sag > 0.9. Non-fast spiking interneurons were classified from a max firing frequency 50-100 Hz, AHP ≥ 12 mV, AP half-width 0.5 to 0.9 ms, sag ratio > 0.9. and max firing frequency 50-100 Hz.

Neurons with a resting membrane potential less negative than -50 mV or a bridge balance higher than 40 MΩ were excluded from the analysis, as were neurons that did not fit within a class from above criteria.

Immunostaining of electrophysiology slices

For identification of cells following recordings, tissue was fixed in 4% PFA overnight at 4°C. Slices were washed with PBS three times, 20 min each, and incubated in Streptavidin-Alexa 488 or Alexa 647 (1:500, Invitrogen) and DAPI (1:1000, in 0.3% PBST) overnight at 4°C. Slices were washed in 0.3% PBST four times and mounted on glass slides with Mowiol® 4-88.

For staining of the interneuron marker parvalbumin (PV), slices were prepared as described above, then incubated in primary antibody solution containing mouse anti-PV (1:1000, PV 235, Swant) and 5% NGS in 0.3% PBST for 48 hrs at 4°C. Slices were then washed and incubated in secondary antibody solution with Alexa-conjugated Streptavidin and DAPI prepared in 0.3% PBST and mounted on glass slides after overnight incubation.

A Zeiss LSM800 microscope was used for image acquisition of the slices. Pinhole was set to 1 Airy Unit. Objectives used include x10 (air), x20 (air) and x40 (oil) to image the hippocampal formation, morphology of biocytin filled cells, and immunolabelling of

interneurons, respectively. To image cell morphology for reconstruction, z-stacks were taken to cover the full slice thickness (1 µm z-step size) and tiling was used to image sufficient volume around the cell for axonal tracing. Cells were reconstructed in Neurolucida® (MBF Bioscience).

Statistics

Statistical tests (Student's t-test, Chi-squared test, Wilcoxon signed rank test) were performed using R (www.r-project.org) 3.6.0, 4.0.0 and 4.0.3-studio. Normality was tested for using both the Shapiro-Wilk test and QQ plots. All data is presented in the format of mean ± SEM unless otherwise stated. A p-value < 0.05 was regarded as significant.

Acknowledgements

We thank Matt Nolan and Nolan Lab for discussions and sharing reagents and equipment. We thank Justus Kebschull for sharing his insight in MAPseq technique, Maria Doitsidou for sharing her equipment and lab space. We also thank Matt Nolan, Klara Gerlei, Brianna Vandrey, Christina Brown and our lab members for critical reading of the manuscript and Gamze Sener for her help with early experiments. This research was supported by a Royal Society and Wellcome Trust Sir Henry Dale fellowship 211236/Z/18/Z.

Contributions

G.S. conceptualised the study, acquired funding and administered the project. G.S. and S.Y.T. performed MAPseq experiments and analysed the data. M.Ö., G.S. and E.S. performed electrophysiology experiments and data analysis. Anatomy and histology experiments were performed and analysed by S.Y.T., G.S., M.Ö., E.S., and M.R.. C.M. developed reagents. Z.B. developed analysis tools and contributed to early discussions. G.S., S.Y.T., E.S. and M.Ö. prepared the original manuscript.

References

1. Marr, D. Simple memory: a theory for archicortex. *Philos. Trans. R. Soc. Lond. B Biol. Sci.* **262**, 23–81 (1971).
2. McClelland, J. L., McNaughton, B. L. & O'Reilly, R. C. Why there are complementary learning systems in the hippocampus and neocortex: insights from the successes and failures of connectionist models of learning and memory. *Psychol. Rev.* **102**, 419 (1995).
3. Koster, R. *et al.* Big-Loop Recurrence within the Hippocampal System Supports Integration of Information across Episodes. *Neuron* **99**, 1342–1354.e6 (2018).
4. Kumaran, D., Hassabis, D. & McClelland, J. L. What Learning Systems do Intelligent Agents Need? Complementary Learning Systems Theory Updated. *Trends Cogn. Sci.* **20**, 512–534 (2016).
5. Schapiro, A. C., Turk-Browne, N. B., Botvinick, M. M. & Norman, K. A. Complementary learning systems within the hippocampus: a neural network modelling approach to reconciling episodic memory with statistical learning. *Philos. Trans. R. Soc. Lond. B Biol. Sci.* **372**, (2017).
6. Sürmeli, G. *et al.* Molecularly Defined Circuitry Reveals Input-Output Segregation in Deep Layers of the Medial Entorhinal Cortex. *Neuron* **88**, 1040–1053 (2015).
7. Czajkowski, R. *et al.* Superficially projecting principal neurons in layer V of medial entorhinal cortex in the rat receive excitatory retrosplenial input. *J. Neurosci.* **33**, 15779–15792 (2013).
8. Beed, P. *et al.* Layer 3 Pyramidal Cells in the Medial Entorhinal Cortex Orchestrate Up-Down States and Entrain the Deep Layers Differentially. *Cell Rep.* **33**, 108470 (2020).
9. Ketz, N., Morkonda, S. G. & O'Reilly, R. C. Theta coordinated error-driven learning in the hippocampus. *PLoS Comput. Biol.* **9**, e1003067 (2013).
10. Witter, M. P. & Amaral, D. G. Entorhinal cortex of the monkey: V. Projections to the dentate gyrus, hippocampus, and subicular complex. *J. Comp. Neurol.* **307**, 437–459 (1991).
11. Köhler, C. A projection from the deep layers of the entorhinal area to the hippocampal formation in the rat brain. *Neurosci. Lett.* **56**, 13–19 (1985).

12. Wozny, C. *et al.* VGLUT2 Functions as a Differential Marker for Hippocampal Output Neurons. *Front. Cell. Neurosci.* **12**, 337 (2018).
13. Rozov, A. *et al.* Processing of Hippocampal Network Activity in the Receiver Network of the Medial Entorhinal Cortex Layer V. *The Journal of Neuroscience* vol. 40 8413–8425 (2020).
14. Naber, P. A., Lopes da Silva, F. H. & Witter, M. P. Reciprocal connections between the entorhinal cortex and hippocampal fields CA1 and the subiculum are in register with the projections from CA1 to the subiculum. *Hippocampus* **11**, 99–104 (2001).
15. Gerfen, C. R., Paletzki, R. & Heintz, N. GENSAT BAC cre-recombinase driver lines to study the functional organization of cerebral cortical and basal ganglia circuits. *Neuron* **80**, 1368–1383 (2013).
16. Kitamura, T. *et al.* Island Cells Control Temporal Association Memory. *Science* vol. 343 896–901 (2014).
17. Tamamaki, N. & Nojyo, Y. Preservation of topography in the connections between the subiculum, field CA1, and the entorhinal cortex in rats. *J. Comp. Neurol.* **353**, 379–390 (1995).
18. Swanson, L. W. & Köhler, C. Anatomical evidence for direct projections from the entorhinal area to the entire cortical mantle in the rat. *J. Neurosci.* **6**, 3010–3023 (1986).
19. Kebschull, J. M. *et al.* High-Throughput Mapping of Single-Neuron Projections by Sequencing of Barcoded RNA. *Neuron* **91**, 975–987 (2016).
20. Petreanu, L., Huber, D., Sobczyk, A. & Svoboda, K. Channelrhodopsin-2–assisted circuit mapping of long-range callosal projections. *Nat. Neurosci.* **10**, 663–668 (2007).
21. Dudman, J. T., Tsay, D. & Siegelbaum, S. A. A role for synaptic inputs at distal dendrites: instructive signals for hippocampal long-term plasticity. *Neuron* **56**, 866–879 (2007).
22. Colgin, L. L. Rhythms of the hippocampal network. *Nature Reviews Neuroscience* vol. 17 239–249 (2016).
23. Wang, Y. *et al.* Fluorescent labeling of both GABAergic and glycinergic neurons in vesicular GABA transporter (VGAT)–Venus transgenic mouse. *Neuroscience* **164**, 1031–1043 (2009).

24. McClure, C., Cole, K. L. H., Wulff, P., Klugmann, M. & Murray, A. J. Production and titering of recombinant adeno-associated viral vectors. *J. Vis. Exp.* e3348 (2011).

25. Murray, A. J. *et al.* Parvalbumin-positive CA1 interneurons are required for spatial working but not for reference memory. *Nat. Neurosci.* **14**, 297–299 (2011).

26. Arber, S., Ladle, D. R., Lin, J. H., Frank, E. & Jessell, T. M. ETS gene Er81 controls the formation of functional connections between group Ia sensory afferents and motor neurons. *Cell* **101**, 485–498 (2000).

27. Cappaert, N. L. M., Van Strien, N. M. & Witter, M. P. Chapter 20 - Hippocampal Formation. in *The Rat Nervous System (Fourth Edition)* (ed. Paxinos, G.) 511–573 (Academic Press, 2015).

28. Pastoll, H., White, M. & Nolan, M. Preparation of parasagittal slices for the investigation of dorsal-ventral organization of the rodent medial entorhinal cortex. *J. Vis. Exp.* (2012) doi:10.3791/3802.

Extended Data Figures

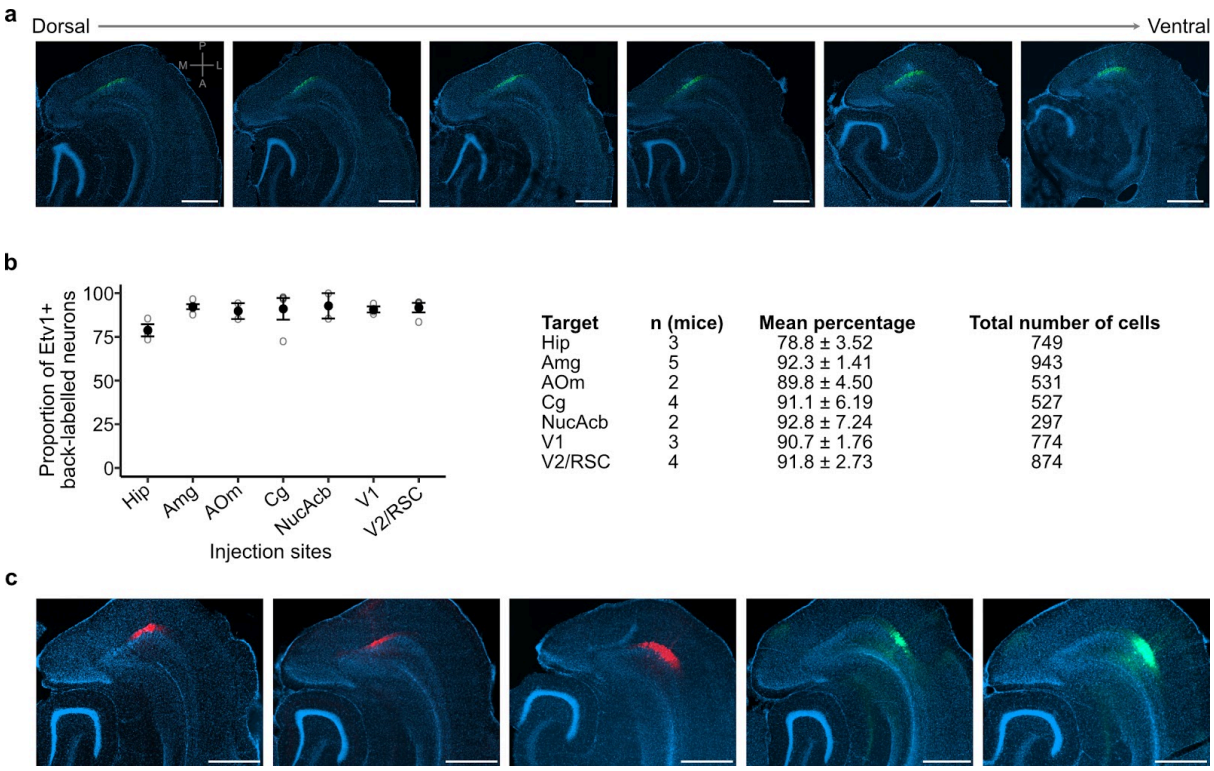

Target	n (mice)	Mean percentage	Total number of cells
Hip	3	78.8 ± 3.52	749
Amg	5	92.3 ± 1.41	943
AOm	2	89.8 ± 4.50	531
Cg	4	91.1 ± 6.19	527
NucAcb	2	92.8 ± 7.24	297
V1	3	90.7 ± 1.76	774
V2/RSC	4	91.8 ± 2.73	874

Extended Data Figure 1. Injection site images and quantification of colocalisation between retrograde markers and Etv1.
a, Horizontal brain sections from a single brain show the dorso-ventral spread of virus-mediated reporter gene expression (Scale bar: 500 µm).
b, Quantification of overlap between retrograde labelling from cortical and subcortical areas and Etv1 expression in L5a of the MEC. The number of mice, mean proportion and total cells counted for each area are shown in the table.
c, Representative injection sites for brains used for quantifying the difference in axon density between proximal and distal CA1 show the medio-lateral extent of injections in the MEC
(Scale bar: 500 µm).

Hip, hippocampus; Amg, amygdala; AOm, medial anterior olfactory area; Cg, cingulate area; NAc, nucleus accumbens; V1, primary visual cortex; V2, secondary visual areas; RSC, retrosplenial cortex.

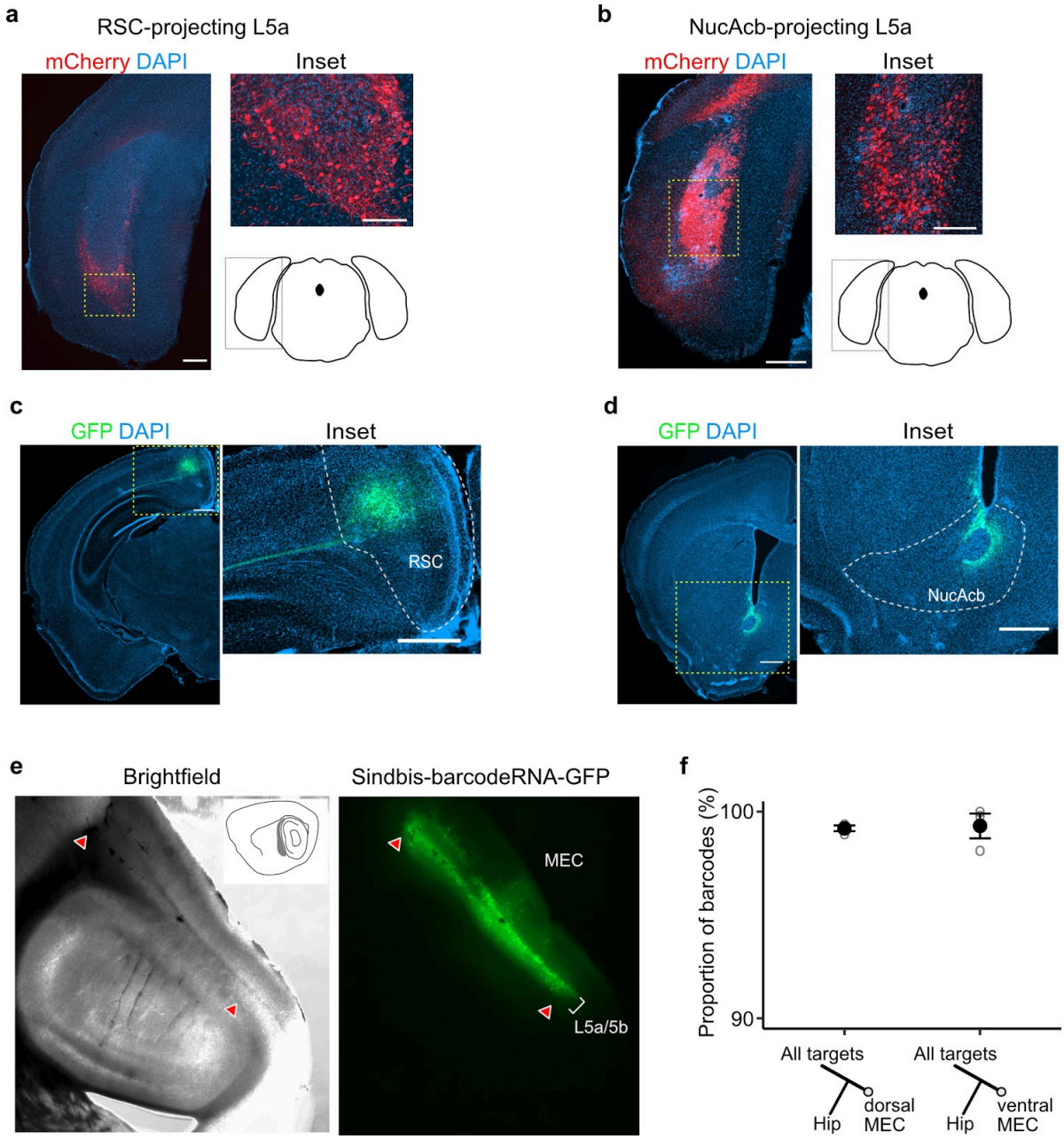

Extended Data Figure 2. Verification of viral expression and further MAPseq data visualisation.
a, b, Coronal brain sections showing labelled neurons in MEC with the combinatorial viral strategy (Scale bar: 500 µm). Inset: high-magnification confocal image of boxed region in left panel showing cell bodies in MEC expressing mCherry.
c, d, Coronal brain sections showing GFP expression at the injection sites in retrosplenial cortex (**d**) or nucleus accumbens (**e**) (Scale bar: 500 µm). Inset: high-magnification of boxed region in left panel.
e, Brightfield and epifluorescence microscope images of the injection site on a sagittal brain section showing the spread of neurons infected by the MAPseq virus library.
f, A neuron's position in the dorso-ventral axis does not affect the likelihood of collateralisation of its axons to the hippocampus (Paired two-tailed Wilcoxon signed rank test, $p = 0.75$, median proportion of collateralizing barcodes in dEC = 98.4%, vEC = 98.9%, n = 3).

RSC, retrosplenial cortex; NucAcb, nucleus accumbens; CNU, cerebral nuclei; Olf/Ctxsp, olfactory and cortical subplate; dHip, dorsal hippocampus; vHip, ventral hippocampus; dMEC, dorsomedial entorhinal cortex; vMEC, ventromedial entorhinal cortex.

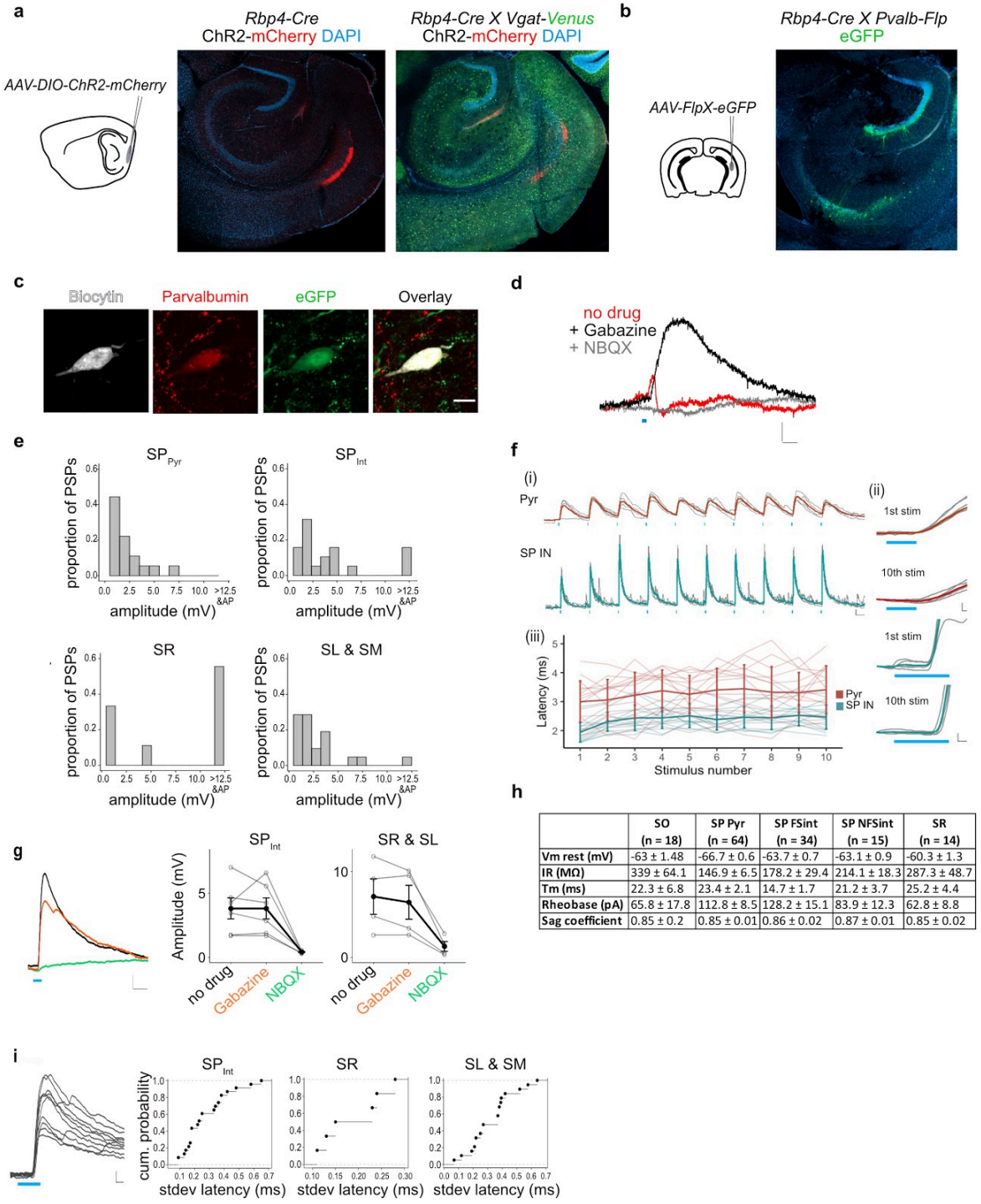

h

	SO (n = 18)	SP Pyr (n = 64)	SP FSint (n = 34)	SP NFSint (n = 15)	SR (n = 14)
Vm rest (mV)	-63 ± 1.48	-66.7 ± 0.6	-63.7 ± 0.7	-63.1 ± 0.9	-60.3 ± 1.3
IR (MΩ)	339 ± 64.1	146.9 ± 6.5	178.2 ± 29.4	214.1 ± 18.3	287.3 ± 48.7
Tm (ms)	22.3 ± 6.8	23.4 ± 2.1	14.7 ± 1.7	21.2 ± 3.7	25.2 ± 4.4
Rheobase (pA)	65.8 ± 17.8	112.8 ± 8.5	128.2 ± 15.1	83.9 ± 12.3	62.8 ± 8.8
Sag coefficient	0.85 ± 0.2	0.85 ± 0.01	0.86 ± 0.02	0.87 ± 0.01	0.85 ± 0.02

Extended Data Figure 3. Experimental design and properties of light responses and responsive neurons

a. Left: Schematic of the injection strategy for delivering virus in the deep EC. Right: Example confocal images of 400 µm horizontal ex-vivo slices showing ChR2-mCherry expression in MEC L5a cells. *Vgat* promoter mediated venus fluorescent protein expression was used for identifying interneurons in CA1 during patch-clamp experiments.

b. Experimental strategy for fluorescence guided patch-clamp recordings made from Parvalbumin expressing neurons. Left: A FlpX-dependent GFP expressing virus was injected in the hippocampus in *Rbp4-CreX Pvalb-Flp* mice. Right: Confocal image of horizontal slice showing labelled interneurons.

c. An example fast-spiking interneuron marked as described in **b**, that showed depolarising PSP upon light stimulation. During recording, the neuron was filled with biocytin and later stained with Streptavidin and Anti-Parvalbumin antibody.

d. An example of a biphasic response recorded from a pyramidal neuron. A late hyperpolarising (red) response was abolished by application of Gabazine to reveal a larger depolarising PSP (black) which was abolished by application of NBQX (grey) (Scale bar: 10 ms, 0.5 mV).

e. Plots showing the frequency distribution of PSP amplitudes in pyramidal neurons and interneurons. PSPs over 12.5 mV were detected in interneurons and often resulted in spiking responses. (SP_{Pyr} : n = 19, SP_{int} : n = 19, SR : n = 9, SL&SM : n = 22 cells)

f. (i) Traces of responses to a train of 10 light stimulation (blue lines), showing relatively stable EPSP amplitude across simulations. (Scale bar: 30 ms, 1 mV) (ii) Magnified images of 1st and 10th pulse illustrate the invariant latency in one example cell (Scale bars: 0.5 ms, 0.5 mV) (iii) Quantification of latency across the train in all cells. Error bars represent SEM.

g. Effects of bath application of Gabazine (orange) and NBQX (green) on PSPs recorded from a fast-spiking pyramidal layer interneuron (left) (Scale bar: 1 mV, 5 ms)**.** Summary quantification of PSP amplitudes for multiple cells (right). The PSP amplitudes were largely unaffected by application of Gabazine (SP_{int} : n = 6 cells, p = 0.99, SR: n = 2 cells & SL n = 2 cells, p = 0.28, 2-tailed Student's t test) but were largely blocked by NBQX (SP_{int} : n = 5 cells, p = 0.03, SR: n = 2 cells & SL n = 2 cells, p = 0.04, 2-tailed Student's t test) indicating AMPA receptor mediated glutamatergic synaptic transmission.

h. Summary table for biophysical properties of neurons used in the study.

i. An example of ten consecutive PSP responses recorded from a single fast-spiking interneuron in SP illustrates the short and invariant latency of PSPs (left). Cumulative probability plots of standard deviation of latencies for neurons with PSP responses that were > 1 mV in amplitude (right). EPSPs of interneurons in all layers except SO had a short latency after light stimulation (mean latency SP: 2.08 ± 0.08 ms, n = 21 cells; SR: 2.00 ± 0.08 ms, n = 6 cells; SL & SM: 2.12 ± 0.21 ms, n = 23 cells). In SO 2 out of 3 of the evoked PSPs had a larger latency of onset (mean latency = 8.5 ± 0.63 ms, n = 2 cells, 2 mice).